2022-01-5004 Published 11 Jan 2022

# Experimental Study of Pressure Coefficients and Flow Field Visualization on a Car Model Based on Shell Eco-marathon Competition Rules

**Salvador Vargas-Díaz and Fredy Alexander Aguirre Gomez** Universidad Libre

**John Jairo Vaca-Rios** Universidade de Sao Paulo Escola de Engenharia de Sao Carlos

**Henry Fernando Osorio** Fundación Universitaria Los Libertadores

***Citation:*** Vargas-Díaz, S., Aguirre Gomez, F.A., Vaca-Rios, J.J., and Osorio, H.F., “Experimental Study of Pressure Coefficients and Flow Field Visualization on a Car Model Based on Shell Eco-marathon Competition Rules,” SAE Technical Paper 2022-01-5004, 2022, doi:10.4271/2022-01-5004.

Received: 04 Mar 2021 Revised: 13 Aug 2021 Accepted: 02 Dec 2021

## Abstract

Aerodynamic efficiency in competition vehicles is considered one of the most important aspects to achieve the best results and turns out to be a fundamental factor in reducing fuel consumption in a vehicle, as is the case with the Shell Eco-marathon Competition. Vehicle aerodynamics has a daily interest in new car prototype design in order to attempt to save fuel. Pressure forces play an important role in car fuel economy and require a detailed study. Wind tunnel experiments play an important role in the study of aerodynamic parameters. The aerodynamics around a vehicle will affect the power, economy, handling stability, and comfort during driving and fuel consumption. In this work, pressure coefficients ($C_p$) at midline around the car model were measured at three different flow speed wind velocities, 14 m/s, 24 m/s, and 30 m/s. Zones with high-, medium-, and low-pressure coefficients were identified on the surface of the vehicle. The low-value $C_p$ found in this study reveals that the geometry of the car model is quite aerodynamic. However the flow visualization showed some areas with turbulence. Drag coefficient based on $C_p$ and unit span length of the car was evaluated, this coefficient was of the order of $9 \times 10^{-2}$.

## Keywords

Car aerodynamics, Shell Eco-marathon Competition, Pressure coefficient, Drag coefficient, Tuft flow visualization

# 1. Introduction

Throughout the history of road cars, it has been observed that their behavior on the track performance depends on aerodynamic forces. However the study of vehicle aerodynamics only began to gain importance in the early 1960s, with the development of the first race car competitions. Since then, this research area has found great advances, and in the last 30 years, these improvements have developed great technological progress in the automotive industry. In the 1970s, the car industry had to face the oil price crisis, for which it was forced to try to minimize the use of fuel for it to be less harmful to the environment, adopting the aerodynamics of the car as an important design parameter among others such as lightweight materials and alternative fuels [1, 2]. To promote the design and development of energy-efficient vehicles, Shell Company, an international energy and petrochemicals corporation, organized an annual event called Shell Eco-marathon Competition for young engineers from around the world. The challenge is to design, build, and drive an energy-efficient vehicle, following the Shell Eco-marathon Official Rules [3].

Aerodynamic aspects must be considered in the design of this type of vehicle, taking into account that the flow over vehicle bodies is mainly turbulence, characterized by complex wake flow, such as recirculation, separation, and long trailing vortex [4]. In the case of the wake studies, Islam et al. [5] showed an unsteady aerodynamics analysis of a squareback and a 40 slant back Windsor body using computational fluid dynamics (CFD) and explores the correlations between the unsteady force coefficients and vortex interaction in the wake. Bonnavion et al. [6] revealed the importance of analyzing the behavior of the wake of a vehicle because they affirm that the control of the wake state with rear side plates improves the drag reduction. The aerodynamics around bluff and streamlined bodies have been widely studied through experimental work and numerical simulation of CFD. Most of these studies have been done on simplified models, such as the Ahmed body [7, 8, 9]. Some studies over realistic car models are also reported in the literature [10, 11]. The study reported by [12] highlighted the importance of conducting wind tunnel tests at different yaw angles in order that the calculated drag faithfully represents the drag experienced by the real vehicle. With this methodology, adequate predictions of the fuel consumption of the prototypes can be expected. Additionally, Bonnavion et al. [13] reported that the influence of lateral wind has to be taken into account as it is almost always present in real driving conditions and has large consequences not only on the drag of the car, thus reducing its fuel efficiency, but also on the lift, therefore modifying its stability. The latter is of importance for the safety of the pilot of the prototypes designed for the Shell Eco-marathon Competition.

Even though a lot of work has been done on the aerodynamics of both prototypes and real car models, every time a new model is designed, it is essential to carry out an aerodynamic study. Therefore, in this work it was proposed to do an experimental study of the proposed model based on the Shell Eco-marathon Competition Rules. During this type of experimental studies, it is required to take measurements of the pressure on the surface of the vehicle to evaluate the aerodynamic forces. Despite the simplicity of pressure taps, they are still used, for example, in wind tunnel testing by Formula 1 (F1) teams. According to Senft et al. [14], the F1 test models are equipped with 500 surface pressure taps on the wing, diffuser, and specific locations. On the other hand, it is well known that there are more sophisticated techniques to identify the flow field in slices located throughout the vehicle, one of them is the Particle Image Velocimetry technique that allows to detect complex vortex structures that are formed downstream of different vehicle structures, such as the front tires. To measure aerodynamic forces, there are balances with multiple degrees of freedom that allow sensing not only the downforce of the entire vehicle but also the front and rear downforce of the vehicle. Regardless of the technological advances of each of these techniques and their costs, Senft et al. [14] indicate that successful F1 teams do not use a technique in isolation and understand the limitations of each technique.

## 2. Motivation

In Shell Eco-marathon Competition, at least three different model geometries have been shown: (1) irregular geometry, (2) drop geometry, and (3) oval geometry. According to the previously proposed geometries, a new prototype design was proposed. The lateral geometry shape (plan view) was based on a symmetrical airfoil (NACA 0035). The upper profile of the side view does not fit into any airfoil according to the Shell Eco-marathon Competition Rules; therefore, a sixth-order polynomial was proposed ($s = a + bx - cx^2 + dx^3 - ex^4 + fx^5 - gx^6$); see Figure 1.

**FIGURE 1** Shell Eco-marathon prototype.



The next challenge was to print a 3D scale model to study experimentally and analyze its aerodynamics in a wind tunnel. Two approaches will be applied, a qualitative approach to determine the behavior of the airflow over the car body by implementing a visualization technique and a quantitative approach to measure the aerodynamic pressure forces by pitot tube manometers.

Drag forces acting over a car body are the consequence of the movement of the flow over the walls of the body. These drag aerodynamic forces directly affect vehicle fuel consumption. The drag force is the sum of perpendicular force (pressure force) over the car surface and the tangential force (shear stress) over the body surface, but the main component of drag force is due to pressure force. The pressure force is observed at the front and the rear of the body. Thus the study of pressure coefficients plays a significant role in understanding car aerodynamics.

## 3. Experimental Setup

In this section we describe the facilities applied on the experimental tests carried out. Two techniques were used: qualitative method (flow visualization) and quantitative method (pressure measurements.

### 3.1. Wind Tunnel Facility

The experiments were carried out in the 0.41 m × 0.61 m × 1.40 m wind tunnel at the Aeronautics Engineering Program at the *Fundación Universitaria Los Libertadores*, Bogota, Colombia; see Figure 2. The cross-sectional area of the test zone is 0.2501 m$^2$. This is an open-loop suction wind tunnel with a test section zone with a high-quality glass wall to facilitate the visualization of the experiment. The range of the air velocity in the tunnel test section is from 5 m/s to 41 m/s. The wind tunnel facility has an entrance section, with a contraction area built of composite materials and with a honeycomb wall of aluminum. Outside of the bottom wall

**FIGURE 2** View of the open-circuit wind tunnel.

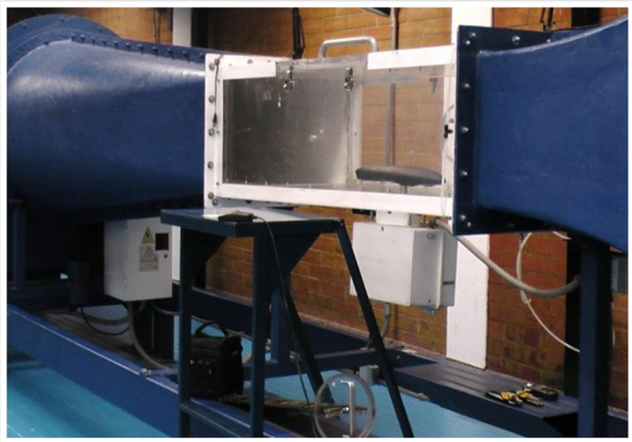



**FIGURE 3** Scale model experimental setup at wind tunnel test section.

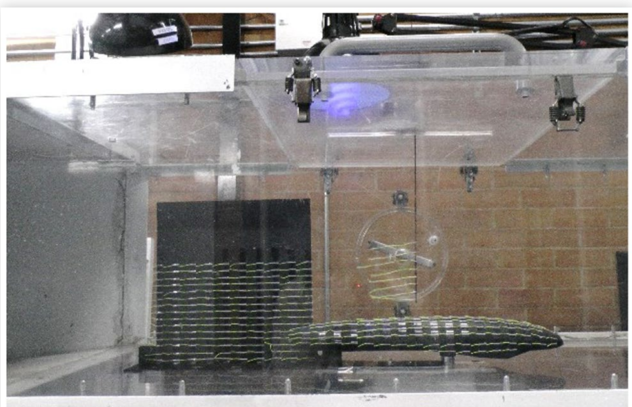



of the wind test zone, a metallic adjustable base is located to fix the model; see Figure 3.

## 3.2. Scaled Car Model

A drawing of the studied scaled car model based on Shell Eco-marathon Competition Rules is shown in Figure 4. The scaling used between the model and the prototype was 1 to 6. As shown in Figure 4, the car model was tested without wheels; this is because, due to the scaling, only a very small part of the wheels (less than 3 mm) were outside of the wheel covers. The maximum cross section in the $X$-axis direction of the model is 0.0058 $m^2$. According to the wind tunnel dimension, the blockage area ratio is 2.32%, which is less than the value of 7.5% recommended by Barlow et al. [15]. The main flow direction is in the $X$-axis, the $Y$-axis is in the vertical direction, and the $Z$-axis is in the horizontal direction, as shown in Figure 4.

For the test series, the car model was mounted through an attachment support located at the middle of the car model as shown in Figure 3. Fourteen holes were made along the longitudinal X-axis of the car model; the holes are distributed as shown in Figure 5(a). The first hole to measure the pressure is located at 30 mm from the front point ($X = 0$). This design allowed the study of pressures both at the top and bottom of the model surface. The holes adaption was made in order to measure the pressure on the upper and bottom sides of the car model; see Figure 5(b).

## 3.3. Surface Pressure Instrumentation

The mean pressure distributions on the car model were measured at the fourteen locations shown in Figure 5. The mean pressure distribution on the top and bottom sides of the car model was taken independently as shown in Figure 6(a) and 6(b), respectively.

A 16-manometer rake was used to measure the mean pressure. The minimum scale used on this U-tube manometer is one millimeter. A total of three lectures were taken until the flow inside the test zone was steady (no more than 10 minutes longer). The manometric liquid used in the experiments is water at 25°C with a density of 997 kg/$m^3$. The measured mean pressure was used to determine the pressure coefficient ($C_p$) defined by Equation 1.

$$C_p = \frac{p - p_{ref}}{0.5\rho V^2} \quad \text{Eq. (1)}$$

where

$p_{ref}$ is the reference pressure
$p$ is the measured pressure
$\rho$ is the fluid density
$V$ is the free stream velocity

**FIGURE 4** Sketch and main dimensions of the car model. (a) Side view and (b) front view.

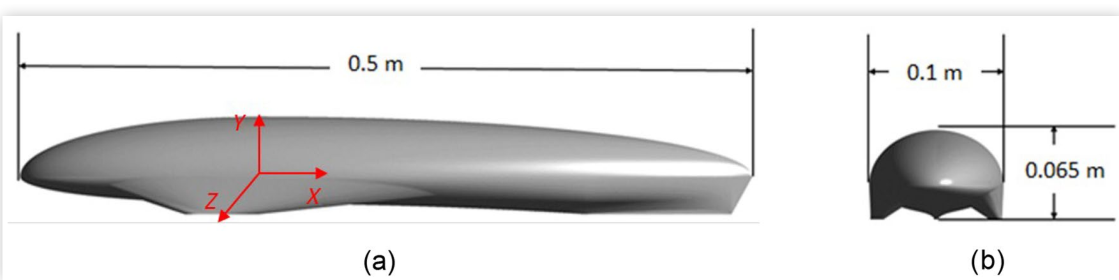

**FIGURE 5** The holes for pressure measurement. (a) Holes location and (b) holes adaption.

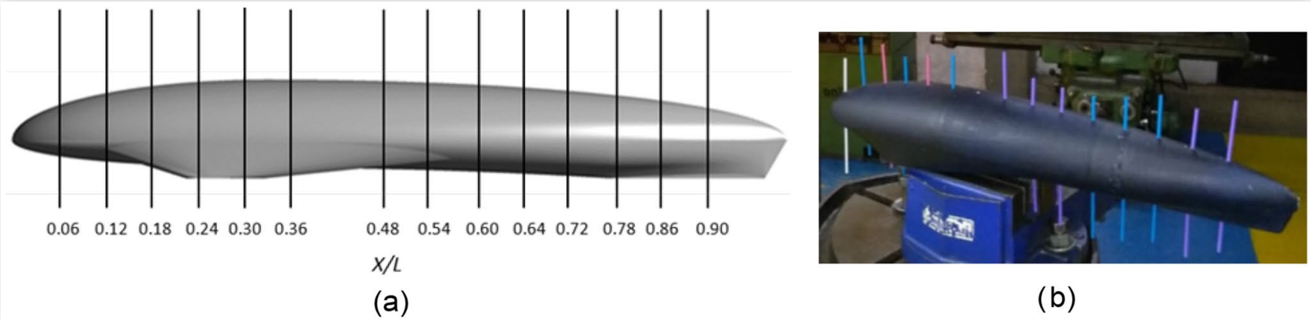




**FIGURE 6** Pressure arrangement used to measure the mean pressure. (a) Top side and (b) bottom side.

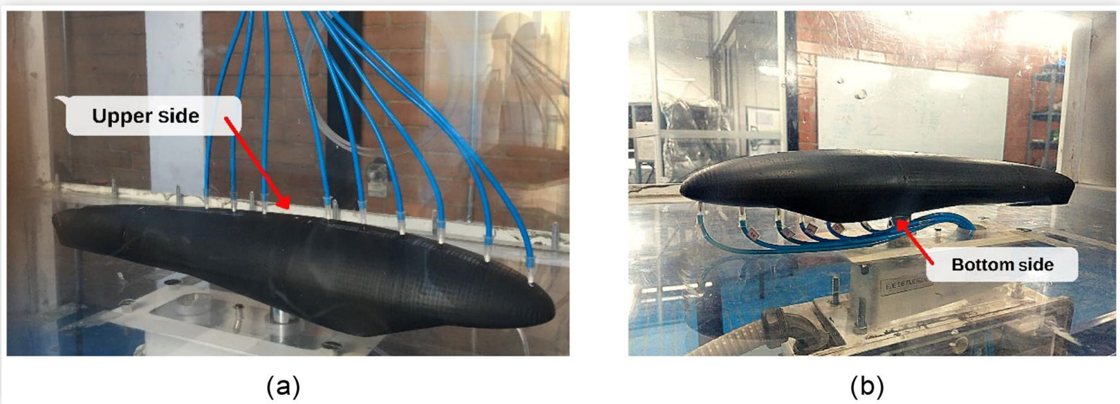




## 3.4. Flow Visualization Instrumentation

Flow field velocity around the car model was analyzed using one of the traditional techniques of flow visualization, tufting technique [16, 17]. For flow visualization the car model was painted in opaque black. On the other side, tuft method is widely used in wind tunnel experiments for a large range of flow velocity to describe qualitatively the surface velocity. Tufts were applied over the entire car model with a mesh of 5 cm × 1 cm. The tuft material is white cotton threads with an estimated length of 5 cm. In order to qualitatively observe the flow field behavior at the rear of the car model, a thin plate with the same mesh pattern of the tufts was placed.

# 4. Results and Discussion

All experiments were carried out under average environmental conditions in the laboratory with a pressure and temperature of 74,900 Pa and 20.5°C, respectively. Three different wind speeds in the wind tunnel were tested, 14 m/s, 24 m/s, and 30 m/s.

## 4.1. Pressure Measurements Results

Mean pressure measurements were obtained at the upper and bottom sides independently. The test series were carried out at Reynolds numbers $2.17 \times 10^5$, $3.73 \times 10^5$, and $4.7 \times 10^5$, based on the length of the car model and fluid properties. With the mean pressure measured, we obtained the $C_p$ using Equation 1. Figure 7(a) shows the upper side $C_p$ for the three different velocities studied in this work. The three $C_p$ curves show the same pattern with no considerable difference, except for the lower velocity on the first half of the car. Higher values of $C_p$ are observed at the front of the car model ($0.1 < C_p < 0.2$). The lowest values are observed at the first half of the car ($-0.3 < C_p < -0.15$). A slight increase in the $C_p$ on the second half of the car is observed ($-0.15 < C_p < -0.1$). On the other side, Figure 7(b) shows the bottom side $C_p$ for the three-speed wind tunnel experiment. From the nose of the car to around 40% of length the car, the values of the $C_p$ remain almost constant ($0 < C_p < -0.1$). In the central part of the car ($0.4 < x/l < 0.8$), a great variation of the $C_p$ is observed ($-0.4 < C_p < 1.5$); this is mainly attributed to the support bar of the model inside the tunnel. Finally, in the rear part of the car model ($0.8 < x/l < 1.0$), the $C_p$ variations observed in the central part of the model begin

**FIGURE 7** Pressure coefficients $C_p$, as a function of model length. Each figure shows two lines, a continuous line corresponding to the upper side and a dashed line corresponding to the bottom side.

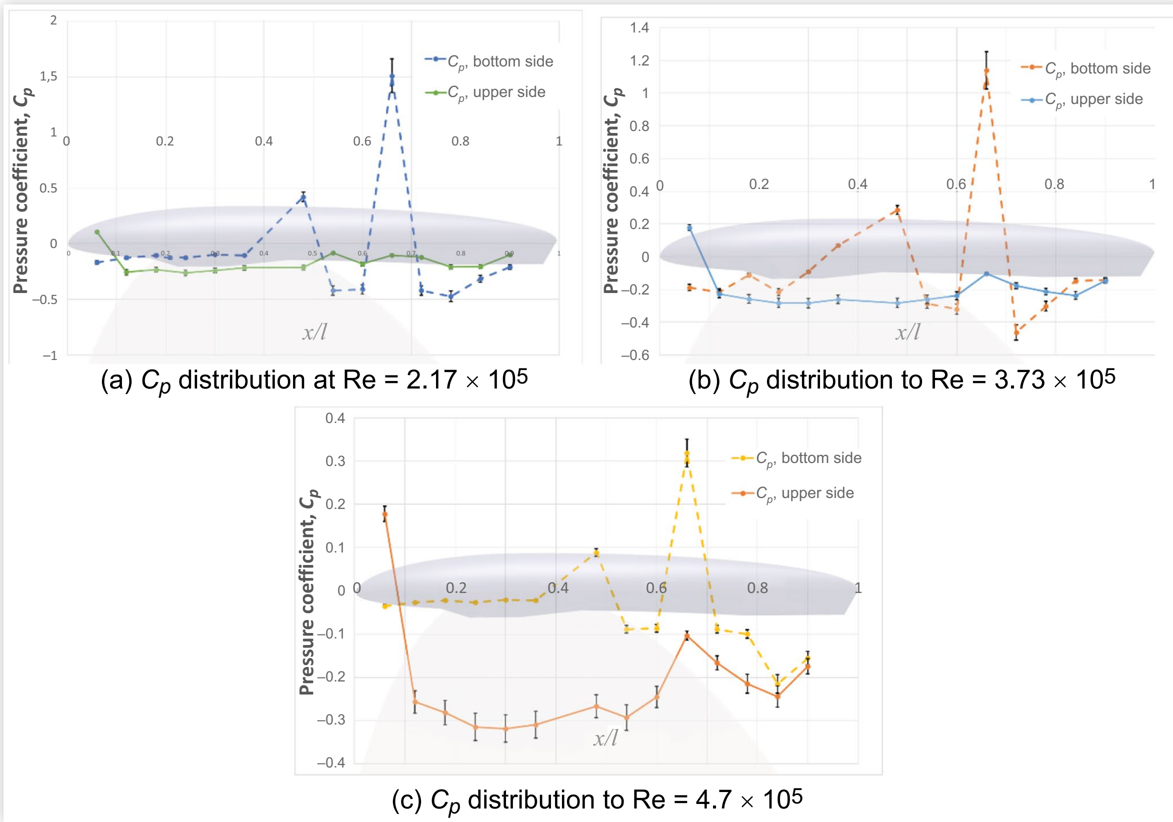


(a) $C_p$ distribution at Re = 2.17 × $10^5$

(b) $C_p$ distribution to Re = 3.73 × $10^5$

(c) $C_p$ distribution to Re = 4.7 × $10^5$



to stabilize ($-0.14 < C_p < -0.15$). The errors found in our experiments agree with those established by Barlow et al. [15] and Stuart [18] where it is reported that the measurement errors when using manometers are around 5%. Our $C_p$ results are reported with the random error bars as shown in Figure 7.

## 4.2. Drag Coefficient Estimation

In this work we calculate the drag coefficient based on the pressure forces measured on the upper and bottom sides of the car model. The friction forces were neglected in this report. The drag coefficient per unit span was calculated applying Equation 2.

$$C_{D,p} = \frac{1}{c}\int_0^c \left( C_{p,u}\frac{dy_u}{dx} - C_{p,b}\frac{dy_b}{dx} \right) dx \qquad \text{Eq. (2)}$$

where

$C_{D,p}$ is the drag coefficient due to pressure
$c$ is the length of the car model
$C_{p,u}$ is the pressure coefficient on the upper side
$C_{p,b}$ is the pressure coefficient on the bottom side
$\frac{dy_u}{dx}$ is the derivative of the upper side
$\frac{dy_b}{dx}$ is the derivative of the bottom side
$dx$ is the derivative in the X-axis (distance between points, $\Delta x = 0.03$ m)

The drag coefficients for three speed wind velocities tested in this work are shown in Table 1. The last line in Table 1, a total drag coefficient over a streamlined body for Reynolds number of the order $10^5$, is also shown in [19].

## 4.3. Flow Visualization

As stated by Russo [20] and Atkins and Boer [21], flow visualization techniques can provide useful qualitative and graphical information understandable immediately without any data processing. Different techniques could be used for different zones in the flow, e.g., over superficies or around the body. Tufts are a technique that can be used either for flow over a surface body or flow field around the body. On the other hand, smoke is a technique in wind tunnel experiments to observe the flow field around a body.

**TABLE 1** Car drag coefficient for different velocities.

| Car model velocity $U$ [m/s] | Drag coefficient/unit span $C_D$ [—] |
|---|---|
| 14 | 0.0085 |
| 24 | 0.0084 |
| 30 | 0.0086 |
| Streamline body | 0.12* |



* Total drag coefficient, $C_D = \frac{F_D}{0.5\rho V^2 S}$.

**FIGURE 8** Flow visualization over a car model using smoke technique, $V$ = 14 m/s.

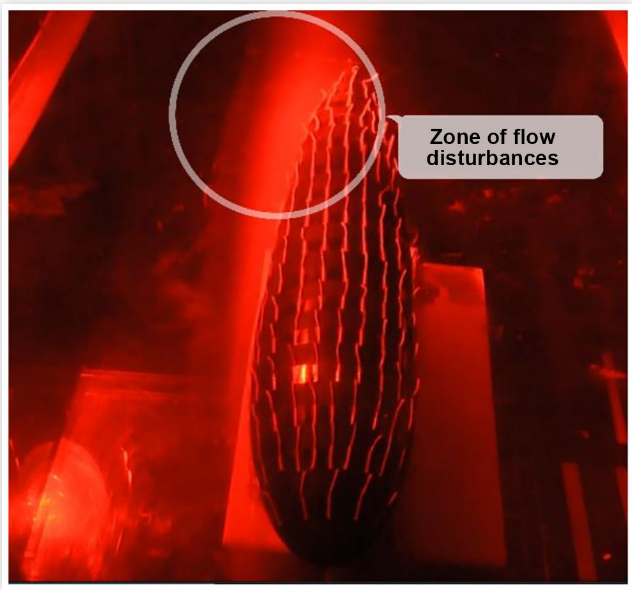




### 4.3.1. Smoke Flow Visualization

Figure 8 shows a top view of the smoke technique used in this work and recommended by [22]. The smoke flow was applied on the left side of the model. Figure 8 shows laminar flow until approximated 80% of the vehicle length. However, in the rear part of the car, flow separation is observed by both tuft and smoke visualizations. The small zone disturbances verified that the geometry design methodology for the proposed prototype using a symmetrical airfoil allows to reduce the form drag coefficient.

### 4.3.2. Tufting Flow Visualization

Flow visualization over the surface of the car model was observed applying the tuft technique. Tuft flow visualization is a common technique used to capture the instantaneous flow patterns [23]. Flow patterns are depicted through tufts orientation with respect to the main flow stream direction. They can reveal flow separation, reattachment points, and recirculation.

**Tufting at the Lateral Side of the Car Body.** As shown in Figure 9(a), no flow disturbances are observed over the car model surface at the front. Figure 9(b) shows the lateral surface, in this zone some disturbances are clearly observed; this vorticity is probably generated by the tire cover. Figure 9(c) and 9(d) show turbulence generated at the rear of the car model, these instabilities over the surface body are due to boundary layer separation.

The smoke technique and tuft technique show an excellent correlation, as shown in Figure 8, and Figure 9(c) and 9(d), zones with flow disturbances due to boundary layer separation.

**Tuft Downstream the Car Body.** In order to observe qualitatively the flow field behind the car model, the tuft technique was applied. A thin plate with a tuft mesh of 5 cm × 1 cm was positioned behind the car. Figure 10 shows an experiment at

**FIGURE 9** Visualization of flow on different important areas of the car model using tufts to a speed wind of 30 m/s.

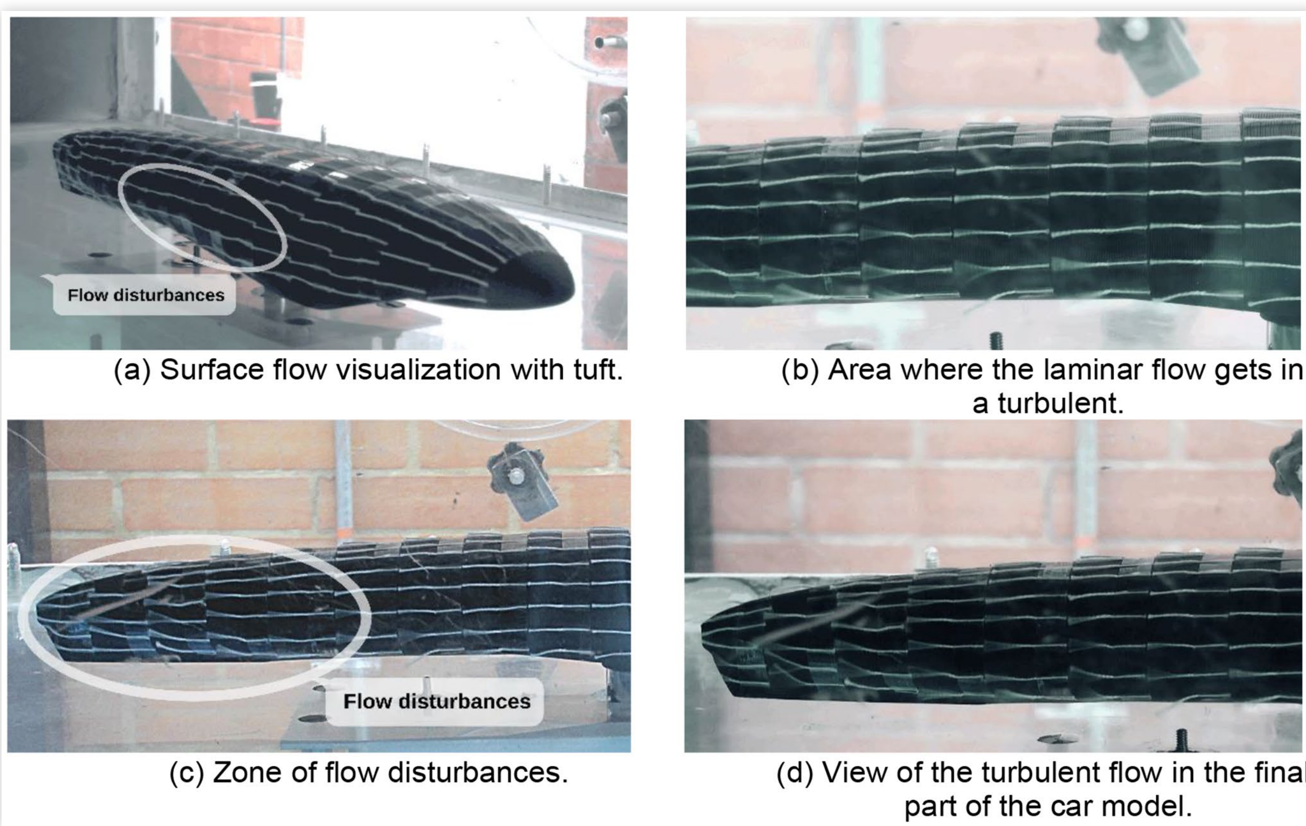

**FIGURE 10** Flow field visualization by the downwash method, behind the car model, $V$ = 30 m/s velocity.

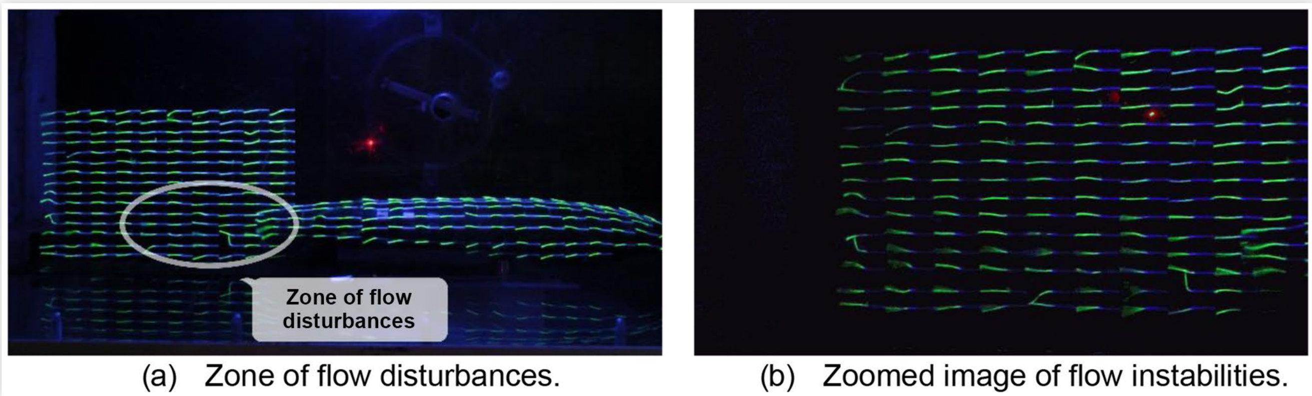




a speed wind of 30 m/s. In this experiment the tufts were painted with a fluorescent liquid, and ultraviolet light was applied. This technique shows a better phenomenon observed behind the car model; however, special care must be taken when painting the threads as this can increase the stiffness of the tufts. In this experiment tufts were made of white cotton threads with a 5 cm length. Figure 10(a) shows turbulent flow close to the ground floor of the test zone. These flow disturbances could be caused by both the vehicle body and the car support. Figure 10(b) shows a zoom in of the disturbances zone. For 14 m/s and 24 m/s flow velocities, flow patterns are like those observed for a 30 m/s velocity.

## 5. Conclusions

In this work we studied experimentally pressure coefficients in a midplane along the main flow direction on a prototype vehicle based on the Official Rules of Shell Eco-marathon Competition. Three different wind tunnel speeds were studied, $2.17 \times 10^5$, $3.73 \times 10^5$, and $4.7 \times 10^5$. Pressure Coefficients results show higher values at the front part of the car model, lower values at the mid-zone, and intermediate values at the rear part. Drag coefficients in 2D were calculated based on the pressure coefficients, a slight change was found with a 1.2% difference between the low and height velocities. By implementing the tuft visualization technique for the surface and flow field, it was possible to identify areas of flow instabilities. In the front area of the vehicle, laminar flow was observed; while in the lateral side and the rear area of the car, flow disturbances were observed. These qualitative findings can be used to make decisions before building the prototype.

It is important to note that the reported drag coefficient does not correspond to the condition that will prevail in the vehicle's driving cycle. This is due to the fact that experiments that do not take into account yaw angles lead to the minimum drag condition and to underestimate the aerodynamic effects of drag on fuel consumption. Therefore, it is advisable to refine the results with tests at different yaw angles that allow including in the analysis the possible effects that the variation of the wind direction would have both in the drag and in a study of efficiency in fuel consumption.

## Acknowledgments

This work was funded by the Research Centre of the Engineering Faculty, (CIFI - Centro de Investigación de la Facultad de Ingeniería) of the Universidad Libre (Colombia), under the project named "Design of a vehicle of low fuel consumption"; code 11030103. All experimental facilities were provided by Fundación Universitaria Los Libertadores, Aeronautical Engineering Program, Bogotá, Colombia

## Contact Information

**John Jairo Vaca-Rios**
jjvacar@usp.br

## References

1. Good, L., Johnson, V., Clough, C., and Lewis, R., "The Aesthetics of Low Drag Vehicles," *SAE Int. J. Engines* 4, no. 2 (2011): 2638-2658, https://doi.org/10.4271/2011-37-0016.
2. Iinuma, Y., Taniguchi, K., and Oshima, M., "Aerodynamics Development for a New EV Hatchback Considering Crosswind Sensitivity," SAE Technical Paper 2018-01-0715, 2018, https://doi.org/10.4271/2018-01-0715.
3. Shell Eco-marathon Competitions, "Shell Eco-marathon 2020 Official Rules," Shell Eco-marathon Competitions, accessed January 2021, https://www.makethefuture.shell/en-gb/shell-eco-marathon.
4. Hucho, W.H., "Aerodynamic Drag of Passenger Cars," in *Aerodynamics of Road Vehicles* (Elsevier: Butterworth-Heinemann, 1987), 106-213, https://doi.org/10.1016/b978-0-7506-1267-8.50008-7.
5. Islam, A., Gaylard, A., and Thornber, B., "A Detailed Statistical Study of Unsteady Wake Dynamics from Automotive Bluff Bodies," *J. Wind Eng. Ind. Aerodyn.* 171 (2017): 161-177, https://doi.org/10.1016/j.jweia.2017.09.009.
6. Bonnavion, G., Cadot, O., Herbert, V., Parpais, S. et al., "Asymmetry and Global Instability of Real Minivans' Wake," *J. Wind Eng. Ind. Aerodyn.* 184 (2019): 77-89, https://doi.org/10.1016/j.jweia.2018.11.006.

7. Morel, T., "Aerodynamics of Road Vehicles," in *Fuel Economy* (1984), 335-392, https://doi.org/10.1007/978-1-4899-2277-9_10.
8. Taiming, H., Xiaodong, Z., Zhongmin, W., and Zhengqi, G., "Experimental and Numerical Investigations of the Vehicle Aerodynamic Drag with Single-Channel Rear Diffuser," *Proceedings of the Institution of Mechanical Engineers, Part D: Journal of Automobile Engineering* 234 (2020): 2216-2227, https://doi.org/10.1177/0954407019893849.
9. Rao, A., Minelli, G., Basara, B., and Krajnović, S., "On the Two Flow States in the Wake of a Hatchback Ahmed Body," *Journal of Wind Engineering and Industrial Aerodynamics* 173 (2018): 262-278, https://doi.org/10.1016/j.jweia.2017.10.021.
10. Zhang, B.F., Zhou, Y., and To, S., "Unsteady Flow Structures around a High-Drag Ahmed Body," *Journal of Fluid Mechanics* 777 (2015): 291-326, https://doi.org/10.1017/jfm.2015.332.
11. Aljure, D.E., Calafell, J., Baez, A., and Oliva, A., "Flow over a Realistic Car Model: Wall Modeled Large Eddy Simulations Assessment and Unsteady Effects," *Journal of Wind Engineering and Industrial Aerodynamics* 174 (2018): 225-240, https://doi.org/10.1016/j.jweia.2017.12.027.
12. Howell, J., Passmore, M., and Windsor, S., "A Drag Coefficient for Test Cycle Application," *SAE Int. J. Passeng. Cars - Mech. Syst.* 11, no. 5 (2018): 447-461, https://doi.org/10.4271/2018-01-0742.
13. Bonnavion, G. et al., "On Multistabilities of Real Car's Wake," *J. Wind Eng. Ind. Aerodyn.* 164 (2017): 22-33, https://doi.org/10.1016/j.jweia.2017.02.004.
14. Senft, V. and Gillan, M.A., "Recent Advances and Test Processes in Automotive and Motorsports Aerodynamic Development," *Proc. Inst. Mech. Eng. Part C J. Mech. Eng. Sci.* 233, no. 23-24 (2019): 7573-7589, https://doi.org/10.1177/0954406219875770.
15. Barlow, J.B., Rae, W.H., and Pope, A., *Low Speed Wind Tunnel Testing*, 3rd ed. (New York: John Wiley & Sons, Inc., 1999), ISBN:0-471-55774-9.
16. Al-Garni, A.M. and Bernal, L.P., "Experimental Study of a Pickup Truck Near Wake," *Journal of Wind Engineering and Industrial Aerodynamics* 98, no. 2 (2010): 100-112, https://doi.org/10.1016/j.jweia.2009.10.001.
17. Azmi, F. and Marzuki, M., "Vehicle Aerodynamics Analysis of a Multipurpose Vehicle Using CFD," *ARPN Journal of Engineering and Applied Sciences* 12 (2017): 2345-2350.
18. Stuart, P.R., "Measurement Uncertainties of U-Tube Manometers and Pressure Balances," *Metrologia* 30, no. 6 (1994): 727.
19. Anderson, J.D. Jr., *Fundamentals of Aerodynamics* (New Delhi, India: Tata McGraw-Hill Education, 2010)
20. Russo, G.P., "Flow Visualization," in *Aerodynamic Measurements* (Woodhead Publishing, 2011), 161-216, https://doi.org/10.1533/9780857093868.161.
21. Atkins, M.D. and Boer, M.F., "Flow Visualization," in *Thermo-Fluidic Measurement Techniques* (Butterworth-Heinemann, 2016), 15-59, https://doi.org/10.1016/b978-0-12-809731-1.00002-2.
22. Mikheev, N.I. and Dushin, N.S., "A Method for Measuring the Dynamics of Velocity Vector Fields in a Turbulent Flow Using Smoke Image-Visualization Videos," *Instruments and Experimental Techniques* 59, no. 6 (2016): 882-889, https://doi.org/10.1134/s0020441216060063.
23. Steinfurth, B., Cura, C., Gehring, J., and Weiss, J., "Tuft Deflection Velocimetry: A Simple Method to Extract Quantitative Flow Field Information," *Experiments in Fluids* 61, no. 6 (2020): 146, https://doi.org/10.1007/s00348-020-02979-7.




ISSN 0148-7191